TECHNICAL MEMORANDUM

277

On the effects of the temporal and spatial sampling of radiation fields on the ECMWF forecasts and analyses

J-J. Morcrette

Research Department

July 1999

European Centre for Medium-Range Weather Forecasts
Europäisches Zentrum für mittelfristige Wettervorhersage
Centre européen pour les prévisions météorologiques à moyen

Abstract

We explore the implications of the temporal and spatial sampling of the radiation fields and tendencies upon the fields produced by the ECMWF system in operational-type forecasts, 4-month seasonal integrations and analyses.

The model is shown to be much more sensitive to economies in the temporal than in the spatial description of the cloud-radiation interactions.

In 10-day forecasts, the anomaly correlation of geopotential shows little sensitivity to a more complete representation of the cloud-radiation interactions, but temperature errors display a stronger dependence to the temporal representation. The difference increases with height, particularly in the tropical areas where interactions between convection, clouds and radiation dominate. In pointwise comparisons over five days, the approximate temporal representation introduces only small differences in total cloudiness, surface temperature, surface radiation and precipitation.

In four-month seasonal simulations, the small errors seen in 10-day forecasts build up and a better temporal resolution of the radiation produces a colder stratosphere through cloud-radiation-convection interactions. The spatial sampling in the radiation computations appears beneficial to the operational model, inasmuch as, close to the surface, it smooths an otherwise wavy radiative forcing linked to the spectral representation of the surface pressure.

Impact of the temporal/spatial sampling in the radiation calculations is usually much weaker in the analyses when and where observational data are available, but can be felt if the density of observations becomes smaller. On the contrary, effect of the temporal/spatial interpolation is important on the sensitivity parameters derived from perpetual July simulations with perturbed SSTs.

1. Introduction

All general circulation models (GCMs) used for climate studies or weather forecasts have a representation of the radiation transfer and a description of the cloudiness, either diagnostic or prognostic. Most, if not all, GCMs also have a simplified description of the cloud-radiation interactions. Due to the computational cost of the various radiation transfer codes, the radiative forcing is usually computed with a smaller time frequency than is used for the dynamics or the other physical processes. In the past, the effect of such economies have already been studied, for models that, at the time, had a diagnostic representation of the cloudiness (Wilson and Mitchell, 1986; Charlock et al., 1988; Smith and Vonder Haar, 1991). In those models, the weak coupling between cloudiness, radiation and the hydrological cycle was leading to an unrealistic variability of the clouds, and of the radiation fields, when compared to satellite data.

Since April 1995, the ECMWF model uses a prognostic representation of the cloudiness (Tiedtke, 1993), in which the time evolution of the cloud elements (cloud water content, cloud area) is directly linked to the various physical processes. However, the full radiation transfer code is only called every 3 hours whereas the time-step for the rest of the model varies from 20 minutes for the operational T_L319 L31 model to 60 minutes for the T_L95 L31 model used for seasonal and longer simulations.

Such a situation for radiation has been prevalent since December 1981, when the ECMWF operational forecast model started to represent the diurnal cycle. The radiation fluxes and tendencies are evaluated at every time-step, but through interpolations, in both time and space, to save computer time and memory. Originally, the full radiation computations were only done every 3 hours from temperature, cloud and humidity fields sampled 1 point out of 4 in the longitudinal direction from the regular model grid using a Fast Fourier Transform method. On this reduced radiation grid, a shortwave (SW) transmissivity was computed at the layer interface by dividing the net SW flux by μ, the cosine of the solar zenith angle at the mid-point of the 3-hour period. Similarly, a longwave (LW) pseudo-emissivity was computed by dividing the net LW flux by σT^4 of the temperature at the layer interface. These transmissivities and pseudo-emissivities were then interpolated to the full model grid using an inverse FFT. For every time-step within the next 3 hours, the net SW and LW fluxes were obtained by multiplying the SW transmissivity by μ and the LW pseudo-emissivity by σT^4 relevant for the time step and grid point.

In the model, presently operational at ECMWF, the full radiation computations are still done every 3 hours (every 1 hour during the first-guess forecasts used as part of the assimilation system or during the first 6 hours of any operational forecast). The net longwave fluxes are now kept fixed for 3 hours whereas the net shortwave fluxes are used as previously indicated. Since September 1991, the operational ECMWF model also uses a reduced horizontal grid for all its computations, keeping roughly the same grid size when going from equator to poles (Hortal and Simmons, 1991). The full radiation computations are carried out on another grid, further sampled, corresponding to all points around the poles decreasing to 1 point out of 4 in the longitudinal direction in the tropics). These full

radiation quantities are then interpolated back using a cubic interpolation scheme to the normal reduced grid, and are then used as discussed above in the temporal interpolation scheme. This approximate treatment therefore makes the radiation fields interact with cloudiness only every 3 hours, and further introduces spatial smoothing of the cloud-radiation interactions.

Given the present resolution of the operational model (T_L319 L31), time step (1200 s), and radiative configuration (full radiation only every 3 hours), the radiation computations account for about 15 percent of the total cost of the model. Accounting for fully interactive radiation at every time-step would increase the time spent in radiation by a factor 9 whereas computing the full radiation fields for all grid-points of the operational reduced grid would increase it by a further factor 3.2.

In the near future, radiation transfer schemes following a neural network approach (Chevallier et al., 1998) may allow radiative transfer computations for a fraction of the computer cost of the present generation of schemes, or computations with a higher spatial/temporal frequency. Therefore, a study of the response of the ECMWF forecast system to a better sampling of radiation is now relevant. The impact of the temporal and spatial interpolation of the radiation fields on the cycle 18r6 L31 version of the model has been studied in a series of experiments, i.e., 10-day forecasts at T_L159, and 4-month simulations at T_L95/T63. We also look at the impact on the operational T_L319 L31 analyses.

In the following, results are presented for the operational configuration (S4T3h), for a model with spatial sampling but full radiation at each time step (S4T1), for a model with no spatial sampling but a 3-hour interval between full radiation computations (S1T3h), and for a model without any spatial nor temporal sampling (S1T1). The ECMWF forecast system is briefly presented in section 2. In section 3, we look at the impact of a better spatio-temporal representation of radiation on 10-day forecasts, whereas, in section 4, we compare surface fields, cloudiness, and precipitation at a number of locations spanning the latitude range from the same forecasts. Section 5 is devoted to the impact on the model climate in 4-month simulations. The impact on analyses is addressed in section 6 and concluding remarks, in particular related to the ECMWF model climate sensitivity, appear in section 7.

2. The ECMWF forecast system

The model used in this study is the so called cycle 18r6 of the ECMWF forecast system, operational since 1 April 1998. The recently revised physics package (Gregory et al., 1998) includes a revised radiation scheme accounting for a more accurate description of the water vapour continuum and ice cloud longwave optical properties consistent in both the longwave and shortwave parts of the spectrum, based on Ebert and Curry (1992). The switching between deep or shallow convection was modified from a test on the moisture convergence to one based on the depth of the convection. The prognostic cloud scheme (Tiedtke, 1993) represents both stratiform and convective clouds, and their time evolution

is defined through two large-scale budget equations for cloud water content and cloud fractional cover. The scheme links the formation of clouds to large-scale ascent, diabatic cooling, boundary-layer turbulence, and their dissipation to adiabatic and diabatic heating, turbulent mixing of cloud air with unsaturated environmental air, and precipitation processes. The results presented in the following sections are obtained with the scheme operationally used for global forecasts and analyses (Jakob, 1994). In the cloud scheme, after an inconsistency in the treatment of absorption of solar radiation had been removed, the original formulation of the fallout of cloud ice of Tiedtke (1993) was reintroduced in the model. The vertical diffusion scheme is now called three times within each model timestep, improving the accuracy of the surface drag coefficient. The dynamical part of the model includes the semi-lagrangian scheme on a linear grid of Hortal (1998). The present ECMWF analysis system is described in Rabier et al. (1997).

3. Impact on 10-day T_L159 L31 forecasts

Starting with a weather forecast perspective, the impact on the objective scores is presented from sets of 12 T_L159 L31 forecasts starting on the 15th of each month over a one year period between September 1997 and August 1998. The impact on the anomaly correlation of Z500, the geopotential at 500 hPa (Fig. 1), is rather small, with a similar result for Z1000 (not shown), indicating that this score is rather insensitive to the details of the cloud-radiation interactions. It is not before day 7 that the different curves begin to be distinguishable, and even then the differences are small. Given that the anomaly correlation is around or below 60 percent at this stage, the time/space sampling has therefore little impact on this objective score. The signal on the temperature mean error is larger (Fig. 2 for T850 and T500, Fig. 3 for T200, and T50). For T850, the signal still reflects the influence of the spatial surface forcing, as seen in the agreement between, on one hand S1T3h and S1T1, on the other hand S4T3h and S4T1. Higher up, the influence of the surface decreases and the influence of the temporal sampling gets bigger: T500, T200 and T50 display a mean error smaller in the T1 forecasts than in the T3h ones, with this effect getting more obvious with height. One could wonder whether this does not simply reflect the fact that the verifying operational analyses through their first-guess forecasts (with a 1-hour full radiation time step) are closer, in terms of cloud-radiation forcing, to the high temporal resolution radiation forecasts (S4T1, S1T1) than to the regular 3-hour full radiation operational forecasts (S4T3h). The impact on the mean temperature error is particularly large in the tropics at 50 hPa (Fig. 3), due to a large increase of the higher level cloud just below the tropical tropopause when radiation is fully evaluated at each time step (see section 5). Results for S4T3h and S1T3h get more and more similar with height, to become almost identical at 50 hPa where clouds do not introduce any more discontinuity in the radiation forcing.

Impact on the wind mean errors at various heights (not shown) is negligible. Apart from this large change in the tropical tropopause temperature, based on such sets of 12 experiments, it would be rather difficult to claim that the model with the most detailed represen-

tation of the cloud-radiation interactions scores significantly better than the operational model.

4. Impact on local surface fluxes and vertical profiles of cloudiness

For pointwise comparisons, we study first the effect of a better temporal representation of the radiative forcing, keeping the same operational spatial representation. For some mid-latitude, tropical and polar locations indicated in Table 1, we compare the surface skin temperature, downward LW radiation, total cloudiness and total precipitation, for 10-day forecasts starting on 1 July 1998 with either the operational version (S4T3h) or the S4T1 version of the T_L159 L31 model. As seen in Figures 4 to 9, the agreement over the first 5 days is generally very good for all four quantities. Whereas the differences in downward longwave radiation (bottom panels of Figs. 4, 6 and 8) obviously reflects the differences in cloudiness (bottom panels of Figs. 5, 7 and 9), the impact on a quantity like surface skin temperature (top panels of Figs. 4, 6 and 8), which somehow integrates the variability in the contributing radiative and turbulent fluxes, is very small. In some instances, the major effect of the better temporal representation of the cloud radiative forcing is a shift in both the starting time of precipitation events as seen in the top panels of Figs. 5, 7, 9. For example, S4T1 precipitation starts earlier than S4T3h over the ARM-SGP location from 18 to 24 hours in the forecast, a similar behaviour is seen at Ilorin for most precipitation events, and at Georg von Neumayer around 66 hours. In mid-latitudes, the S4T1 precipitation events are often more intense but of a shorter duration: The ARM-SGP precipitation around 20 hours reaches 3.4 mm/hour for 1 hour with S4T1 whereas S4T3h only gives a maximum of 2 mm/hour but the event lasts longer, so that accumulated over the 3 relevant hours S4T1 precipitation is 3.39 mm and S4T3h precipitation is 3.42 mm. In more convective atmospheres, S4T1 precipitation is usually larger than S4T3h precipitation but no clear signal on the duration of events is found (Fig. 7).

The impact on the vertical profiles is more difficult to assess, as a change in advection (either horizontal and/or vertical) might also contribute to a change in the distribution of the cloud elements over a given location. Here, we compare profiles of cloud fraction and longwave radiative heating given by S4T3h and S4T1 for five days over three locations somewhat spanning the climatological spectrum: over Payerne (Fig. 10), Kwajalein (Fig. 11), where deep convection prevails on the ocean, and over the South Pole (Fig. 12). Overall the structure of the cloudiness and therefore of the radiative heating rates (both LW and SW) are very similar between the two configurations. From these figures and similar ones over the other locations, it is clear that the S4T3h radiative forcing, which varies step-wise every 3 hours, obviously gives less smooth cloud fields. However, whether this contributes to an increase or a decrease in cloudiness at a given level is difficult to assess, specially at high- and mid-latitudes, where travelling perturbations dominate the temporal variations in cloudiness. In the tropical area, where interaction between convection, cloud and radiation is much stronger, and horizontal advection is smaller, the small differences seen over the first 5 days obviously accumulate and clearly show up in the seasonally long integrations.

Even if the impact of a better spatial representation of the radiative forcing on objective scores appears very small (see section 3), the local impact on local meteorological features is noticeable. For example, land-sea contrast, properly represented in all physical processes but the radiation, can be seen to improve with S1T3h relative to S4T3h. At the interface between warm land surface and colder ocean surface, like around the Mauritania coast, the low cloudiness is positioned closer to the coast in the S1T3h and S1T1 simulations.

5. Impact in seasonal integrations

It is only when comparing results on a longer time-scale that the slightly different cloud-radiative forcing translates into sizeable differences in most model fields. A series of T_L95 L31 simulations was run with the different spatial/temporal configurations for the summer of 1987. Each set includes six 4-month simulations starting 24 hours apart from 26 April to 1 May 1987 and all finishing on 1 September 1987. Such ensembles of experiments have been shown by Brankovic et al. (1994) to be large enough to give a reasonable level of statistical significance.

Figures 13 to 16 present results averaged over the last 3 months of the simulations (between 1 May and 31 August 1987). Systematic differences are apparent in zonal mean cloudiness (Fig. 13), temperature (Fig. 14), relative humidity (Fig. 15) and specific humidity (Fig. 16). As already seen in the 5-day forecast results over Kwajalein, the convection seems to be particularly sensitive to the frequency of the full radiation computations. Compared to the operational configuration (S4T3h), the S4T1 and S1T1 fields show a large increase in tropical upper level cloudiness and humidity. Given that most of this increase is located over the ocean, a mechanism such as discussed, for example, by Betts and Ridgway (1988) appears at work in the model. In the S1 configurations, the radiative cooling in the descending branch is slightly increased relative to S4T3h (through slighly larger longwave cooling and slightly smaller shortwave heating). Above the PBL, this extra radiative cooling is balanced by a slightly larger adiabatic descending motion. In the tropical oceanic PBL, the atmosphere is slightly drier, which enhances the latent heat flux. The additional mositure is brought to the ITCZ where it feeds a slightly stronger convection. The convective mass-flux scheme (Tiedtke, 1989) tends to detrain mostly right at the tropopause level. This results in an increase in the upper level clouds (anvil-type clouds), with a slight temperature increase below, either linked to the direct convective heating or more likely to an enhanced greenhouse effect by the additional high-level clouds. The emitting source at low temperature provided by these high clouds contributes to the observed cooling of the stratosphere at these latitudes, mainly through a decrease of the absorption by ozone. This cooling is then spread dynamically to higher latitudes.

All three modified configurations show an increased temperature in the northern hemisphere northward of 30 °. However, following a statistical significance analysis, the only feature to be above the 0.99 confidence level is in fact the tropical decrease in specific humidity around 90 hPa.

Table 2 compares the low- (for $\sigma > 0.8$), middle- (between $\sigma = 0.45$ and $\sigma = 0.8$), high-level (for $\sigma < 0.45$), et total cloudiness, for the different configurations with the normal cloud scheme, and for the different configurations with the cloud scheme without the cloud production term proportional to the longwave radiative cooling. First result is the large impact of that term on the production of low- to middle-level clouds (about 6 and 5 percent respectively, whatever the spatio-temporal configuration). Second, although there are some systematic differences between the different configurations, with the radiation at every time step leading to larger high-level and total cloud amounts, the signals remain rather small on a global basis. Moreover, most of the differences brought by the different configurations do not appear at specified locations.

When looking at surface fluxes, one can see the benefit brought by the linear grid approach of Hortal (1998). Figure 17 compares the surface net longwave flux for the 4 types of experiments discussed above (S4T3h, S4T1, S1T3h, and S1T1), for a spectral model with a T63 truncation and the more recent T_L95 equivalent from the point of view of the physical calculations but with more terms in computing the dynamical tendencies. When full radiation is computed for all grid-points, the spectral nature of the model is apparent in all physical fields through a modulation of the surface pressure. This in turn affects the vertical column of the various absorbers and finally shows up as a (slight) modulation of the fields. This effect is particularly evident in the surface net longwave radiation (presented in Fig. 17), but also in the surface net shortwave radiation (not shown). In this respect, the linear grid approach significantly reduces this problem of orographic ripples, but does not make it fully disappear. It must be noticed that the radiation configuration used for the operational forecasts at ECMWF with its S4 horizontal sampling hides the problem. By providing a smoother spatial radiative forcing, this configuration also smooths out other physical fluxes and tendencies.

6. Impact on operational analyses

The operational analyses rely on 6-hour first-guess forecasts, for which the full radiation is called every hour, so that the direct effect of the temporal interpolation discussed above is three times smaller. We carried out a series of analyses from 19989630 18UTC to 19980706 18UTC with the operational T_L319 L31 model including all four radiation configurations. Given the forcing by observations, the impact of the various radiation configurations is very much smaller than in the free-running 10-day forecasts and 4-month simulations. However, where (or when, as it is sometimes the case at 06 or 18 UTC) the density of observations gets smaller, the influence of the first-guess forecast gets larger. The impact on cloudiness, temperature and specific humidity is presented as zonal means in Figures 18 to 20. Obviously the major impact, in both specific humidity and temperature, is seen where the density of observations is low like over Antarctica, and to a lesser extent in the northern polar region. In these areas, the differences between the various configurations can be as high as 0.15 K in temperature and 5 % in relative humidity. Otherwise, over the rest of the atmosphere, the impact on the zonal means of temperature and humidity remains quite small, with maximum differences occuring in the upper part of the

ITCZ, reaching at most 0.05 K in temperature, and 2 % in relative humidity over patchy areas showing no particular organization.

Although the cloudiness is not an analyzed quantity, the changes in analyzed humidity and temperature have an impact on the cloudiness. Cloudiness over Antarctica displays variations up to 5 % depending on the configuration. Otherwise, the upper troposphere in the equatorial region shows up as the most sensitive area to these small changes in analyzed moisture and temperature with a maximum decrease of 2 % in zonal mean cloudiness around 200 hPa.

7. Concluding remarks and climate sensitivity

To conclude this topics and to put in perspective the differences introduced by the radiation temporal/spatial interpolation scheme, the signal is usually smaller than the signal seen when changing details of the cloud microphysical processes, cloud radiative properties or cloud overlap assumptions. At present, in a weather forecast environment, the huge increase in computer time introduced by decreasing the time frequency and/or spatial sampling of the full radiation computations could only become acceptable if these computations were handled with a much more efficient method, such as the neural network approach (Chevallier et al., 1998).

The main conclusions are the following:

- the model appears much more sensitive to economies in the temporal than in the spatial description of the cloud-radiation interactions;

- in terms of the 10-day forecast quality, the anomaly correlation of geopotental displays little sensitivity to the spatial/temporal representation;

- the configuration presently used for running the operational data assimilation introduces little bias on the results of the analyses;

- in seasonal simulations, the impact is much stronger with the increase in temporal resolution leading to a decrease in upper tropospheric moisture in the tropics, a larger amount of tropical high clouds, and a colder stratosphere, whereas the increase in spatial resolution increases the temperature only slightly over most of the troposphere .

All results presented here are specific to the ECMWF model. The question is whether the ECMWF model might be more or less sensitive to the temporal (and spatial) interpolation than other general circulation models are. Studies by Wilson and Mitchell (1986), Charlock et al., (1988), Smith and Vonder Haar (1991) indicated that the weak coupling between cloudiness, radiation, and the hydrological cycle, existing in models with a diagnostic cloud scheme, overestimated the variability of top of the atmosphere radiation fluxes when compared to satellite observations of the radiation budget. Tiedtke (1994) showed that the prognostic cloud representation, with a much stronger coupling to the

cloudiness to the physical processes, was more likely to improve the time continuity of the cloud fields, particularly with respect to the anvil-topped convective cloud systems.

However, the prognostic cloud scheme relates the formation, maintenance and dissipation of cloud volume and cloud water to most parts of the physics package, thus including radiation, might make the ECMWF model more sensitive to the radiation interpolation scheme than a model with clouds diagnostically derived from relative humidity, or clouds whose water content is prognosed but cloud fraction is still diagnosed from relative humidity. As such, relative humidity is a much smoother quantity in both time and space than most of the outputs of the dynamical and physical processes used as precursors/predictors of cloud volume and cloud water in the ECMWF scheme. However, the effect of the temporal interpolation described here are likely to be found in other weather forecast or climate models, as most models cannot afford a radiation scheme fully interactive with the rest of the physical parametrizations.

As seen in sections 5 and 6, the intertropical high troposphere is the area where the largest changes in temperature, humidity and cloudiness occur when changing the configuration of the radiation computations. So we looked at the impact of the temporal/spatial interpolation scheme on the sensitivity of the model to a change in sea surface temperature computed following the procedure outlined in Cess et al. (1990). A number of T_L95 L31 simulations were performed for the 4 temporal/spatial configurations for perpetual July 1987 conditions, with fixed SST with a plus or minus 2 K increment, and fixed sea ice, soil moisture and snow cover maintained at 19870701 conditions. The clear and total sky feedback and sensitivity parameters for the 4 configurations used here are presented in Table 3. A simple interpretation of these results is that, through higher spatial and temporal resolution, the cloudiness, and therefore, the top of the atmosphere radiation fields are more likely to follow the intensification of the convective activity brought by the increased sea surface temperature over the ocean, thus increasing the sensitivity parameter. This result also shows how sensitive Cess's methodology is to what can be thought of as relatively intricate details of the cloud-radiation interactions, and as such, at least in the context of the ECMWF model, casts doubt on the validity of the exercise.

Acknowledgments

Drs. Anton Beljaars and Martin Miller are thanked for reviewing the manuscript.

References

Brankovic, C., T.N. Palmer, and L. Ferranti, 1994: Predictability of seasonal atmospheric variations. J. Climate, 7, 217-237.

Cess, R.D., G.L. Potter, J.-P. Blanchet, G.J. Boer, M. Deque, W.L. Gates,S.J. Ghan, J.T. Kiehl, H. Le Treut, Z.X. Li, X.-Z. Liang, B.J. McAvaney, V.P. Meleshko, J.F.B. Mitchell, J.-J. Morcrette, D.A. Randall, L. Rikus, E. Roeckner, J.-F. Royer, U. Schlese, D.A. Sheinin, A. Slingo, A.P. Sokolov, K.E. Taylor, W.M. Washington, R.T. Wetherald, andI. Yagai, 1990: Intercomparison and interpretation of climate feedback processes in seventeen atmospheric general circulation models. J. Geophys. Res. 95D, 16,601-16,617.

Charlock, T.P., K.M. Cattany-Carnes, F. Rose, 1988: Fluctuation statistics of outgoing longwave radiation in a general circulation model and in satellite data. Mon. Wea. Rev., 116, 1540-1554.

Chevallier, F., F. Cheruy, Z.-X. Li and N. A. Scott, 1998: A neural network-based approach for the longwave radiative computations of a General Circulation Model. Geophys. Res. Letters, submitted.

Ebert, E.E., and J.A. Curry, 1992: A parametrisation of ice cloud optical properties for climate models. J. Geophys. Res., 97D, 3831-3836.

Gregory, D., J.-J. Morcrette, C. Jakob, and A. Beljaars, 1998: Introduction of revised radiation, convection and vertical diffusion schemes intp cycle 18r3 of the ECMWF integrated forecasting system. ECMWF Technical Memorandum No. 254., 39 pp.

Hortal, M., and A.J. Simmons, 1991: Use of reduced Gaussian grids in spectral models. Mon. Wea. Rev., 119, 1057-1074.

Hortal, M., 1998: TL319 resolution and revised orographies. ECMWF Research Department Memorandum, R60.5/MH/23, 9 March 1998, 18 pp.

Jakob, C., 1994: The impact of the new cloud scheme on ECMWF's Integrated Forecast System. Proceedings of ECMWF Workshop on "Modelling, Validation and Assimilation of Clouds", 277-294.

Morcrette, J.-J., 1991: Evaluation of model-generated cloudiness: Satellite observed and model-generated diurnal variability of brightness temperature. Mon. Wea. Rev., 119, 1205-1224.

Rabier, F., J.-F. Mahfouf, M. Fisher, H, Jarvinen, A. Simmons, E. Andersson, F. Bouttier, P. Courtier, M. Hamrud, J. Haseler, A. Hollingsworth, L. Isaksen, E. Klinker, S. Saarinen, C. Temperton, J.-N. Thepaut, P. Unden, and D. Vasiljevic, 1997: Recent experimentation on 4D-Var and first results from a simplified Kalman filter. ECMWF Technical Report 240, 42 pp.

Smith, L.D., and T.H. Vonder Haar, 1991: Cloud-radiation interactions in a general circulation model: Impact upon the planetary radiation balance. J. Geophys. Res., 96D, 893-914.

Tiedtke, M., 1993: Representation of clouds in large-scale models. Mon. Wea. Rev., 121, 3040-3061.

Tiedtke, M., 1994: Critical aspects of cloud parametrization in large-scale models. Proceedings of ECMWF Workshop on "Modelling, Validation and Assimilation of Clouds", 22-42.

Wilson, C.A., and J.F.B. Mitchell, 1986: Diurnal variation and cloud in a general circulation model. Quart. J. Roy. Meteor. Soc., 112, 347-369.

TABLE 1. Locations for the pointwise comparisons

Location	Latitude	Longitude
Regina	50.12 N	104.43 W
Payerne	46.82 N	6.95 E
ARM-SGP Billings	36.37 N	97.30 W
Kwajalein	8.72 N	167.73 E
Ilorin	8.32 N	4.34 E
Florianopolis	27.58 S	48.52 W
Syowa	69.00 S	39.35 W
Georg von Neumayer	70.39 S	8.15 W
South Pole	89.98 S	24.48 W

TABLE 2. Cloud cover at various levels with the different spatio-temporal configurations and two versions of the cloud scheme

	S4T3h	S4T1	S1T3h	S1T1
Reference				
HCC	35.95	36.13	35.92	36.60
MCC	26.38	26.40	26.74	26.41
LCC	23.76	23.39	23.68	23.74
TCC	62.17	62.27	62.40	62.83
No LW				
HCC	34.57	34.94	34.00	34.95
MCC	21.88	21.41	21.75	21.40
LCC	17.57	17.52	17.00	17.28
TCC	55.26	55.35	54.51	55.07

TABLE 3. Feedback and sensitivity parameters derived from T_L95 L31 perpetual July simulations

Configuration	clear-sky	total sky	ratio
S4T3h	0.504	0.657	1.304
S4T1	0.476	0.767	1.611
S1T3h	0.461	0.693	1.504
S1T1	0.452	0.777	1.718

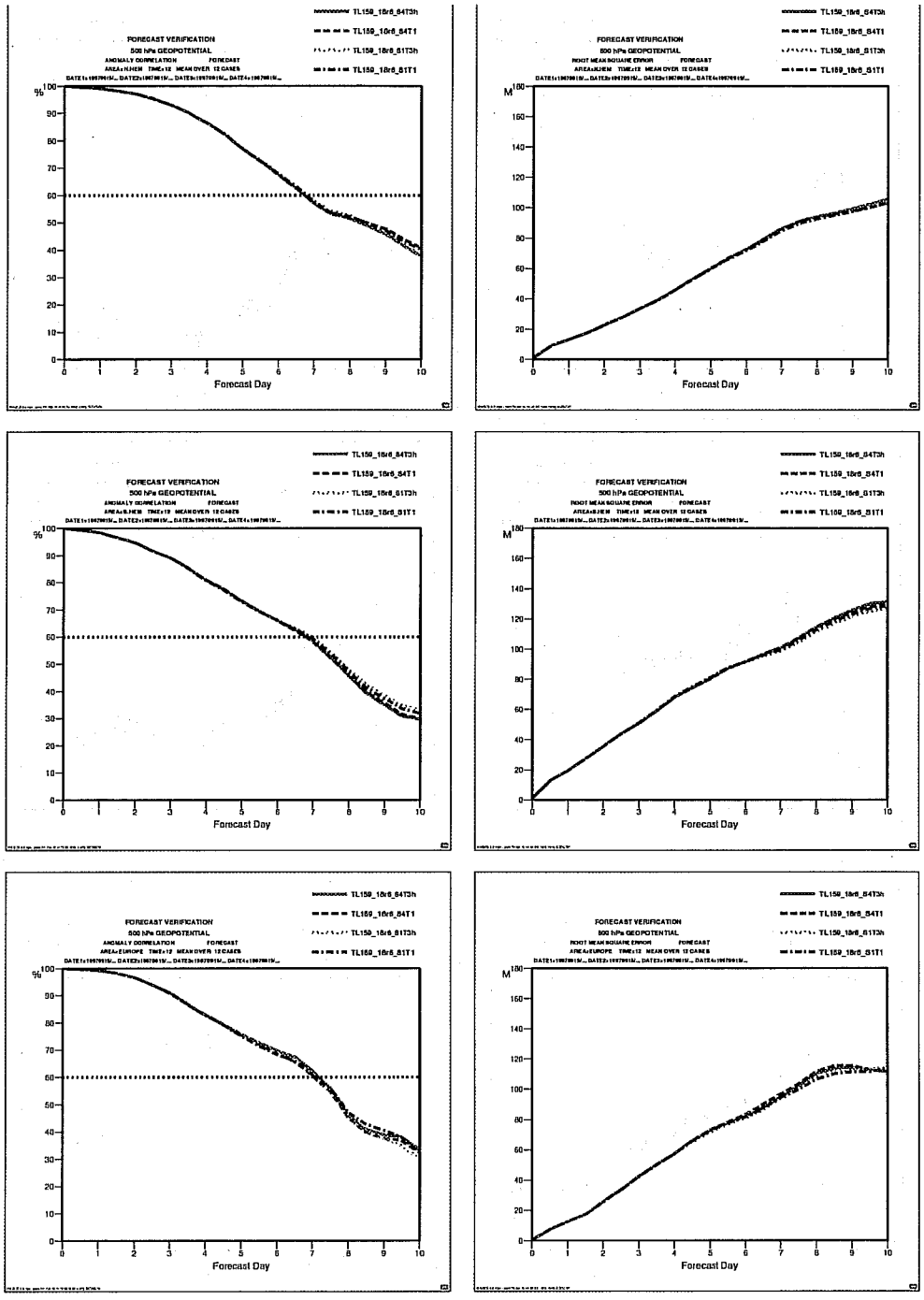

Figure 1: The anomaly correlation and r.m.s. error of the geopotential at 500 hPa for the various time-space configurations for the Northern (top panels) and Southern (middle panels) hemispheres, and the tropical region (bottom panels). Full line is S4T3h, long dash line is S4T1, dotted line is S1T3h, and dot-dash line is S1T1.

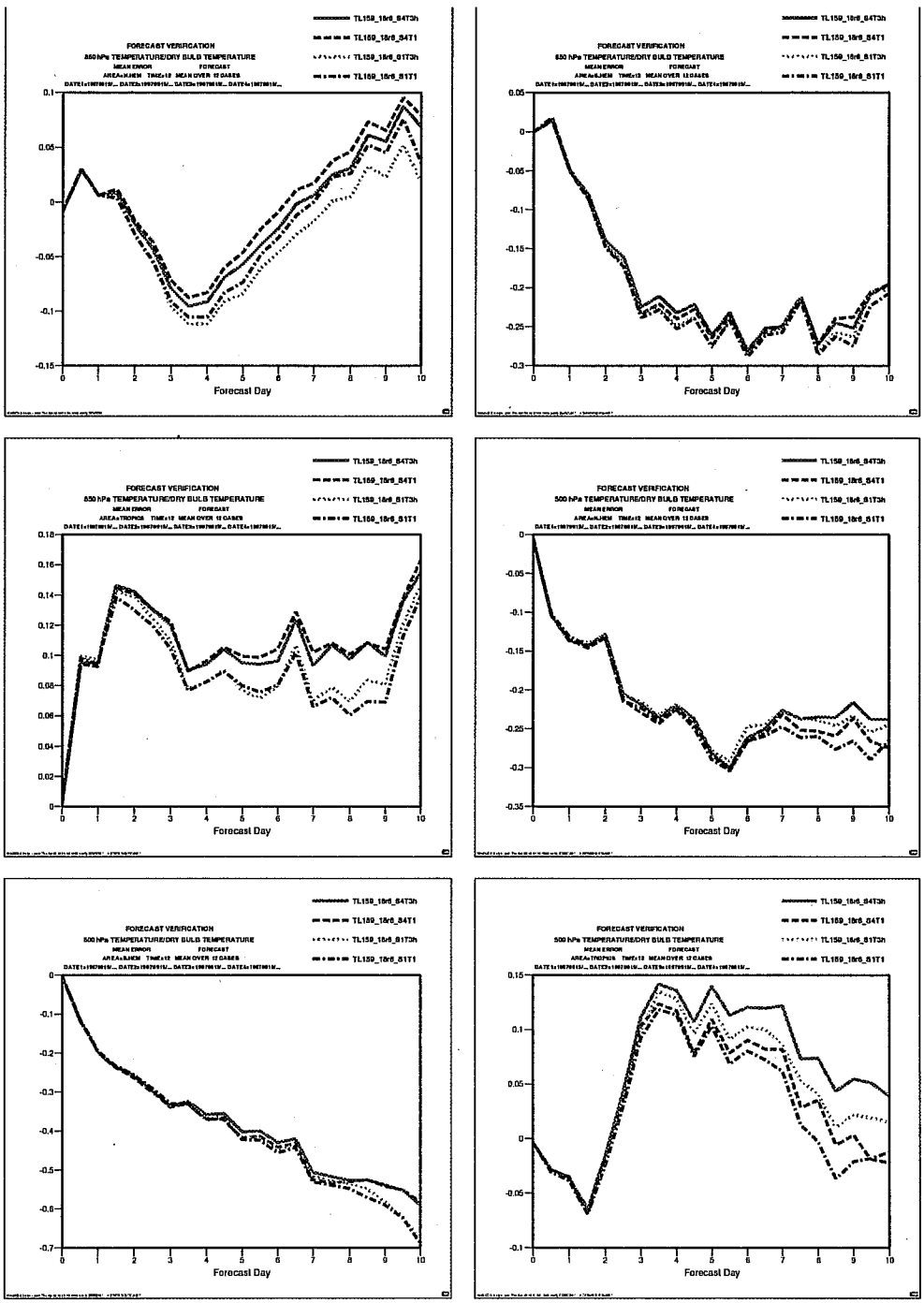

Figure 2: The mean error of the temperature at 850 and 500 hPa for the various time-space configurations for the Northern and Southern hemispheres, and the tropical region. Panels are read from left to right, and top to bottom.

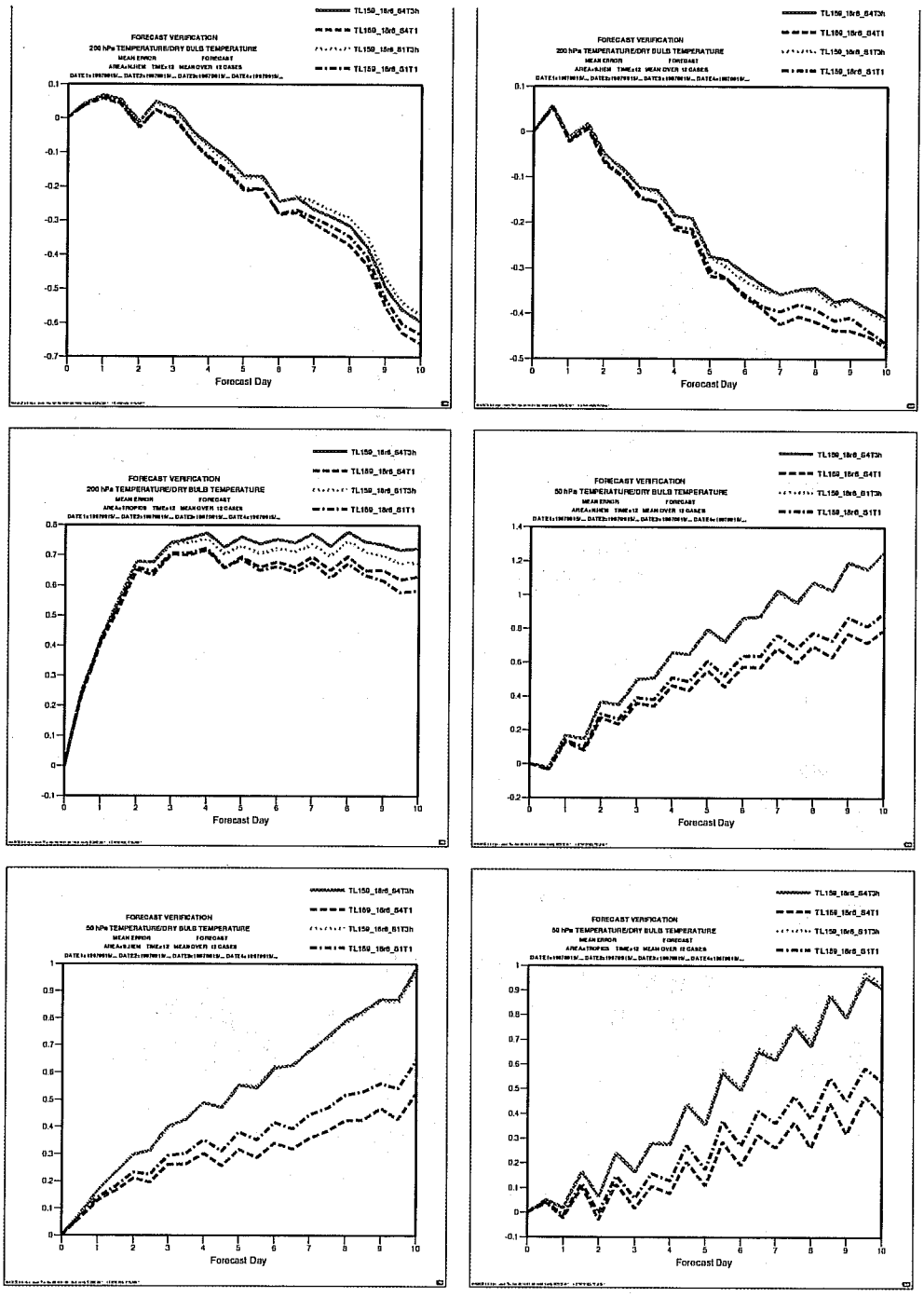

Figure 3: As in Figure 2, but for the mean error of the temperature at 200 and 50 hPa.

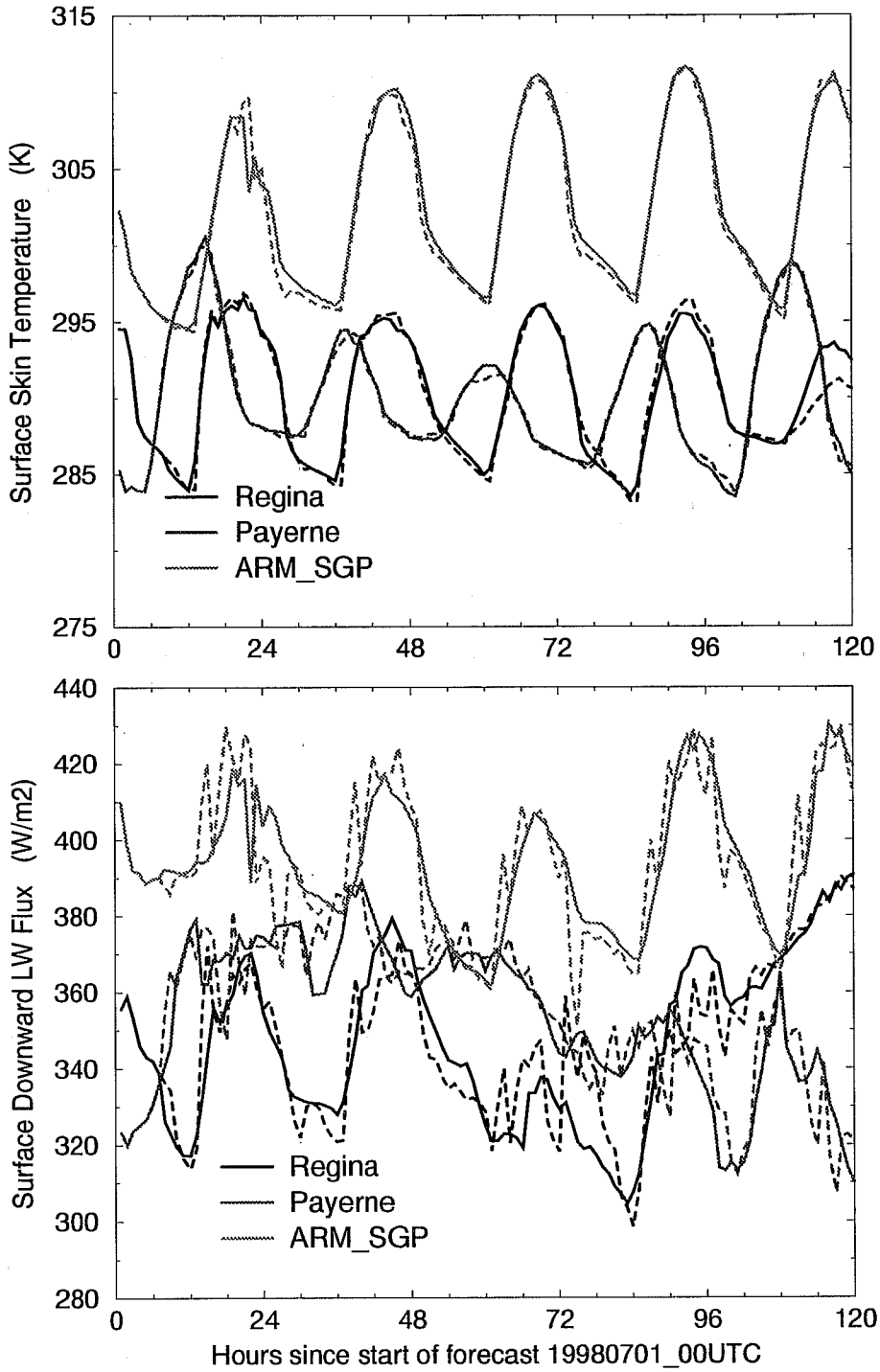

Figure 4: The surface skin temperature (top) and downward longwave radiation (bottom) over the first 5 days of T_L159 L31 forecasts with full radiation computations either every 3 hours (full line) or every time-step (20 mn; dash line) for the first 3 locations of Table 1.

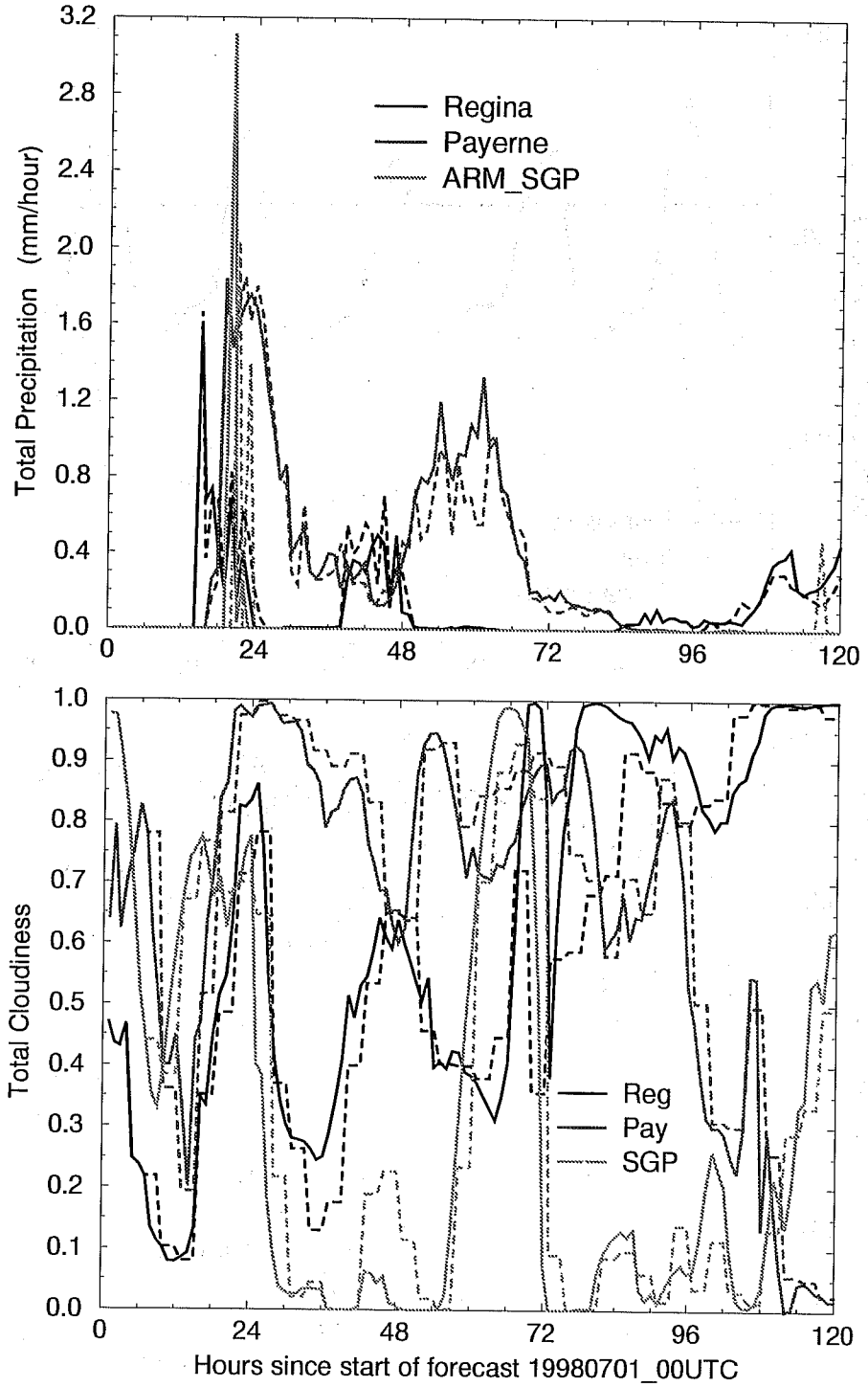

Figure 5: As in Figure 4, but for the total precipitation and the total cloudiness.

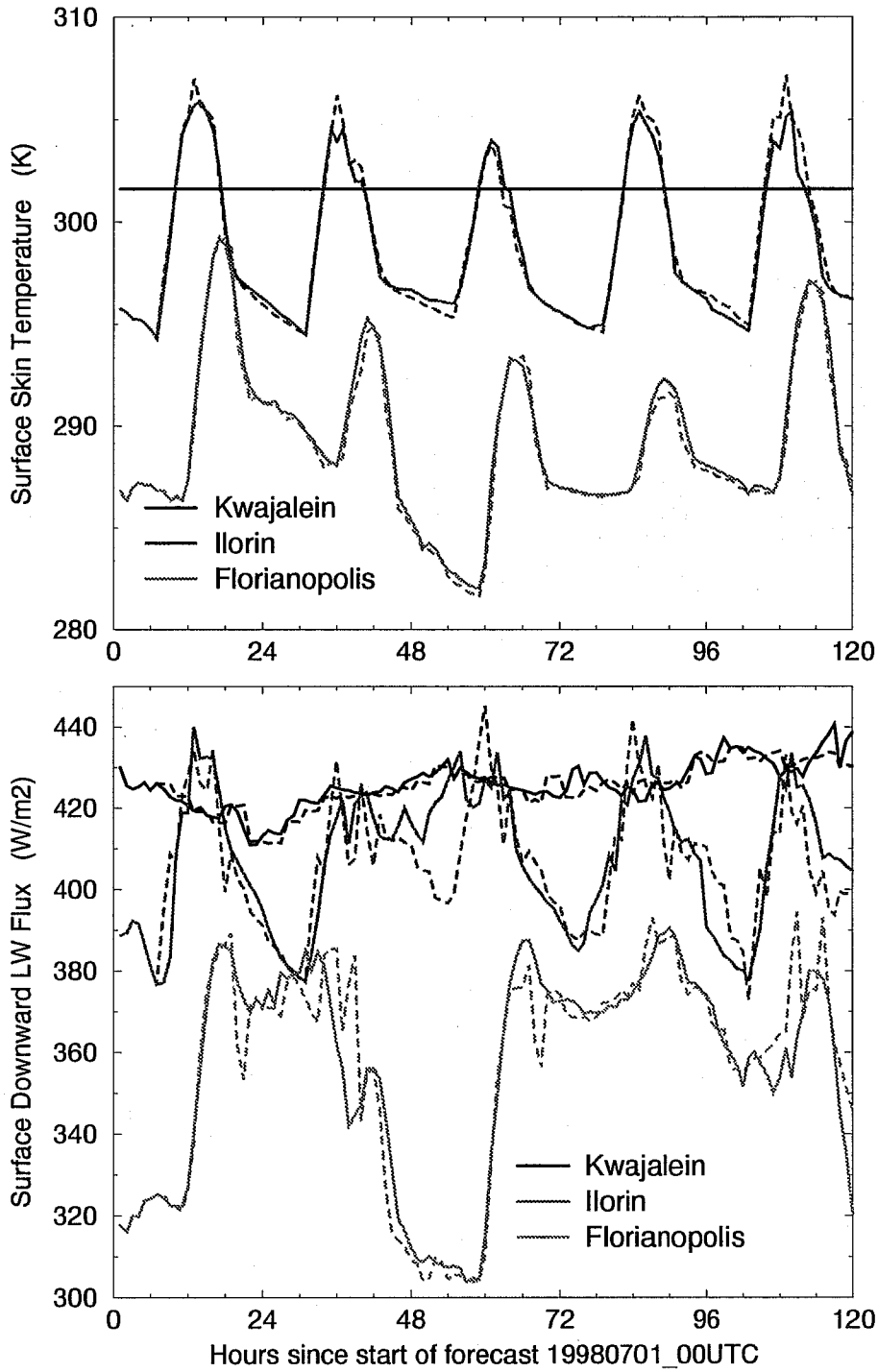

Figure 6: As in Figure 4, but for the 3 tropical locations of Table 1.

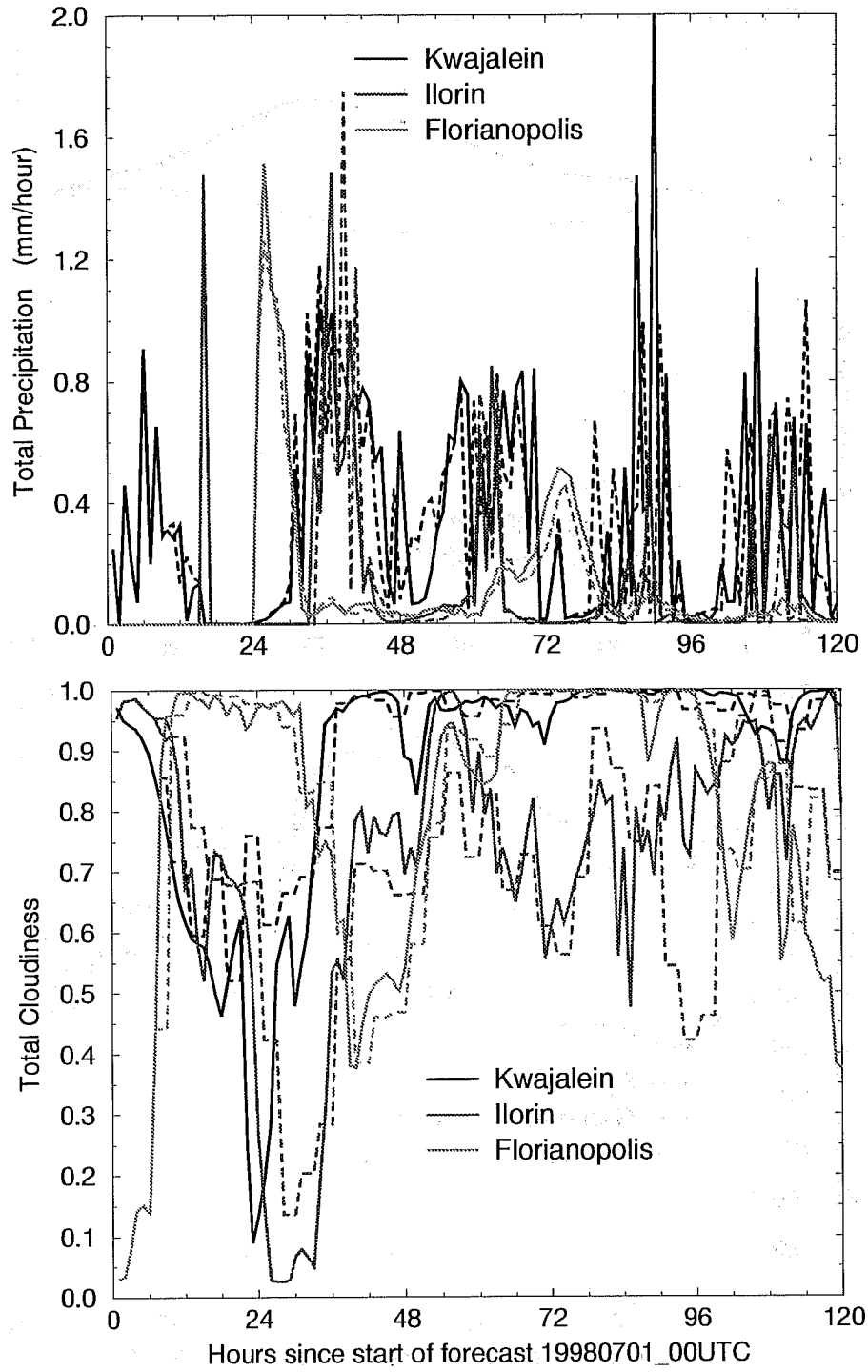

Figure 7: As in Figure 5, for the 3 tropical locations of Table 1.

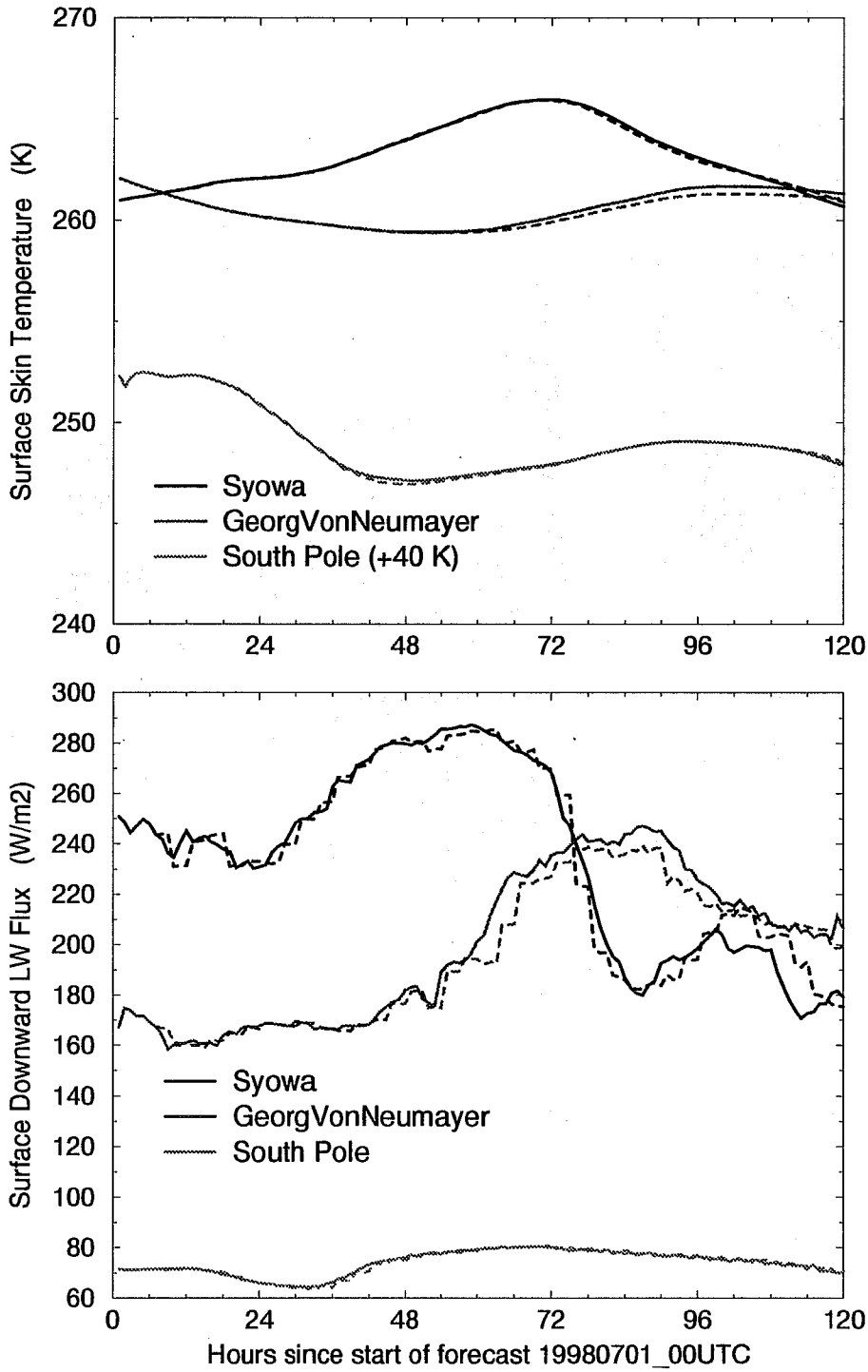

Figure 8: As in Figure 4, for the 3 polar locations of Table 1

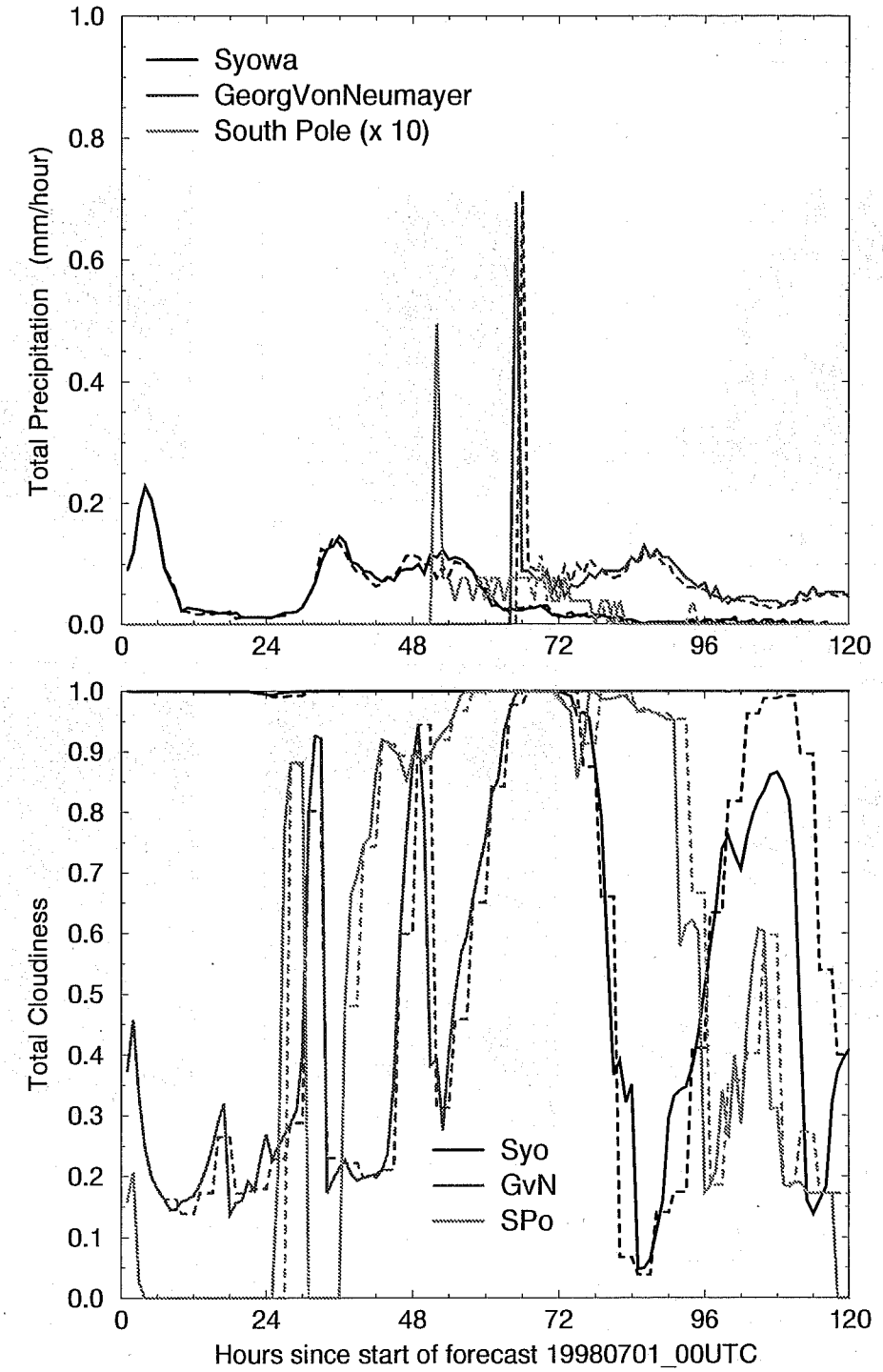

Figure 9: As in Figure 5, for the 3 polar locations. of Table 1.

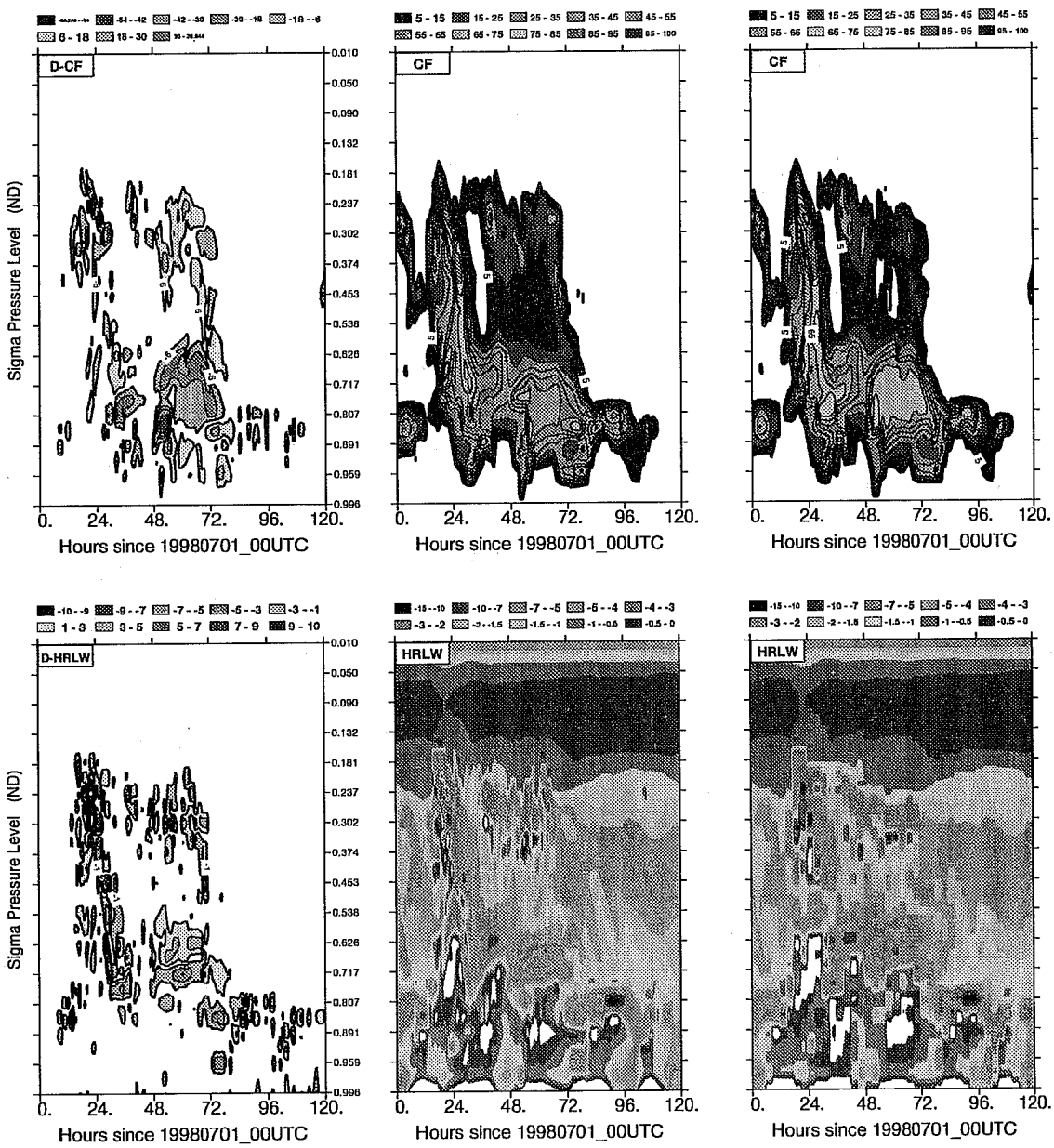

Figure 10: The evolution of the vertical distribution of the cloud fraction (top panels, in percent) and of the longwave heating rate (bottom panels, in K/day) over Payerne during the first 5 days of the T_L159 L31 forecasts. Left panels show the difference S4T1-S4T3h (step is 12 percent for D-CF, 2 K/day for D-HRLW), middle panels are S4T1, right panels are S4T3h (step is 10 percent for CF, whereas limits for HRLW are 0,- 0.5, -1., -1.5, -2, -3, -4, -5, -7, -10 and -15 K/day

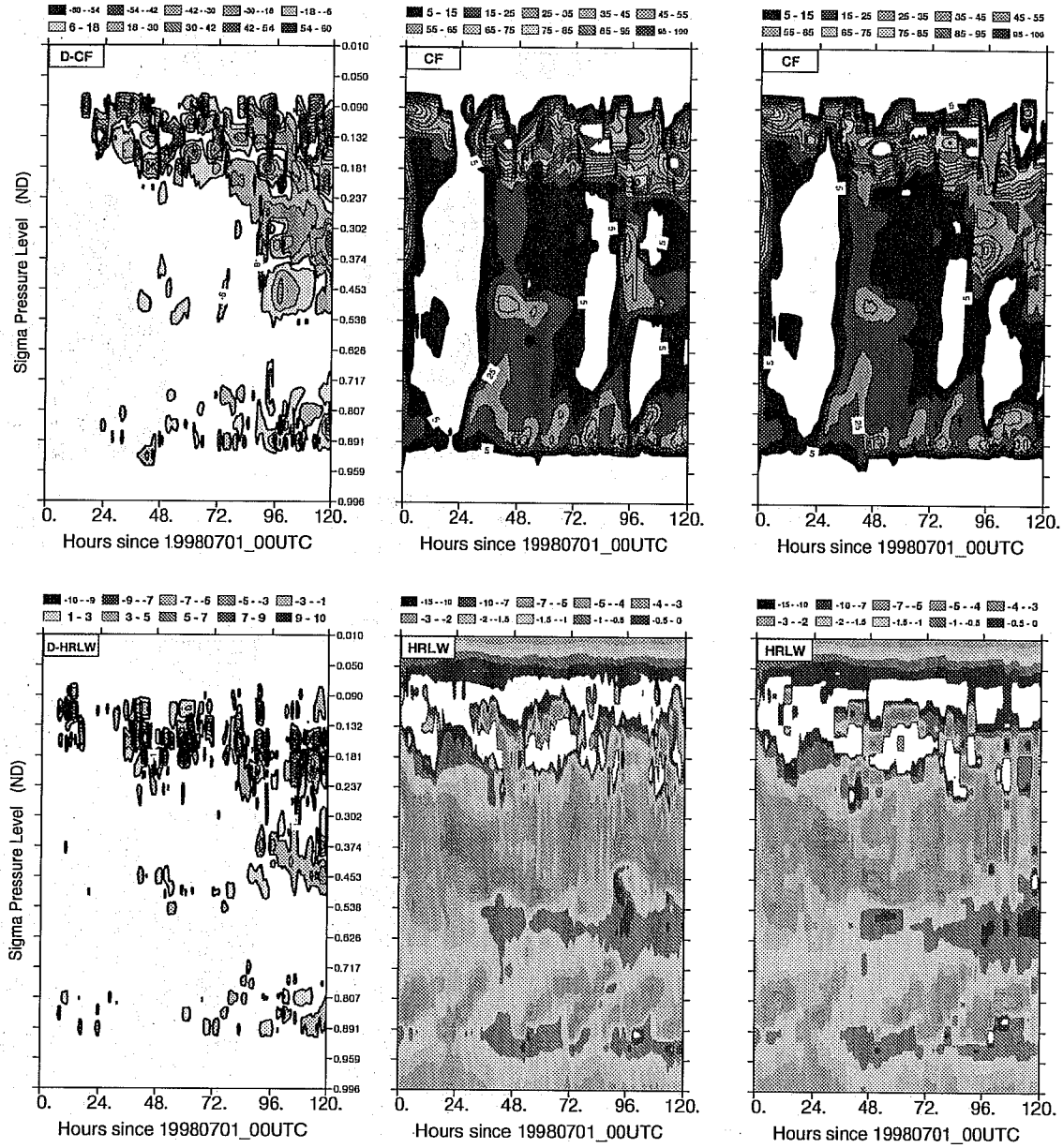

Figure 11: As in Figure 10, but for the cloud fraction and the LW heating rate over Kwajalein.

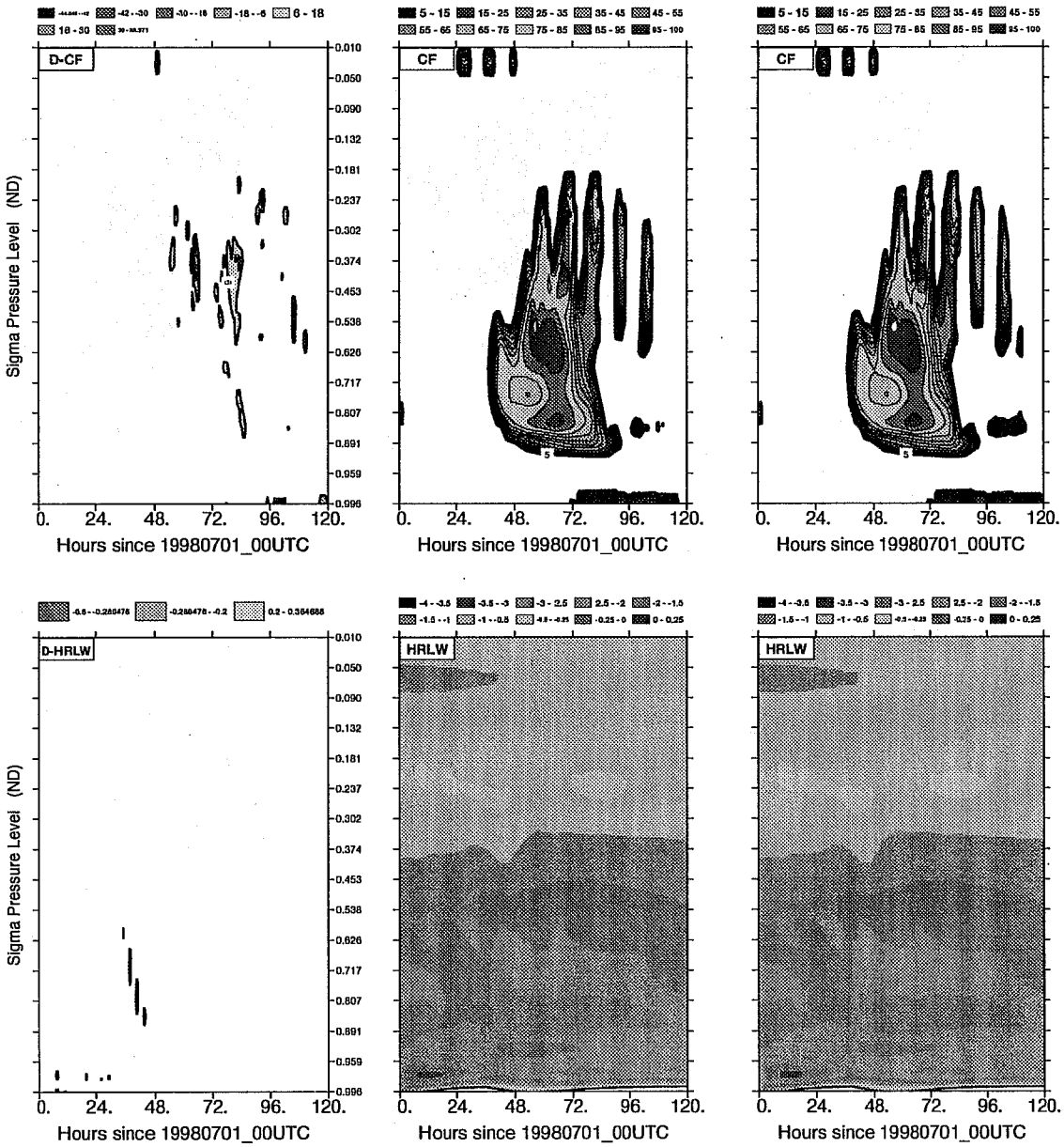

Figure 12: As in Figure 10, but for the cloud fraction and the LW heating rate over the South Pole. For the LW heating rate, the scale is different from that in Figs. 10 and 11 (limits for HRLW are 0.25, 0, -0.25, -0.5, then a -0.5.step to -4 K/day).

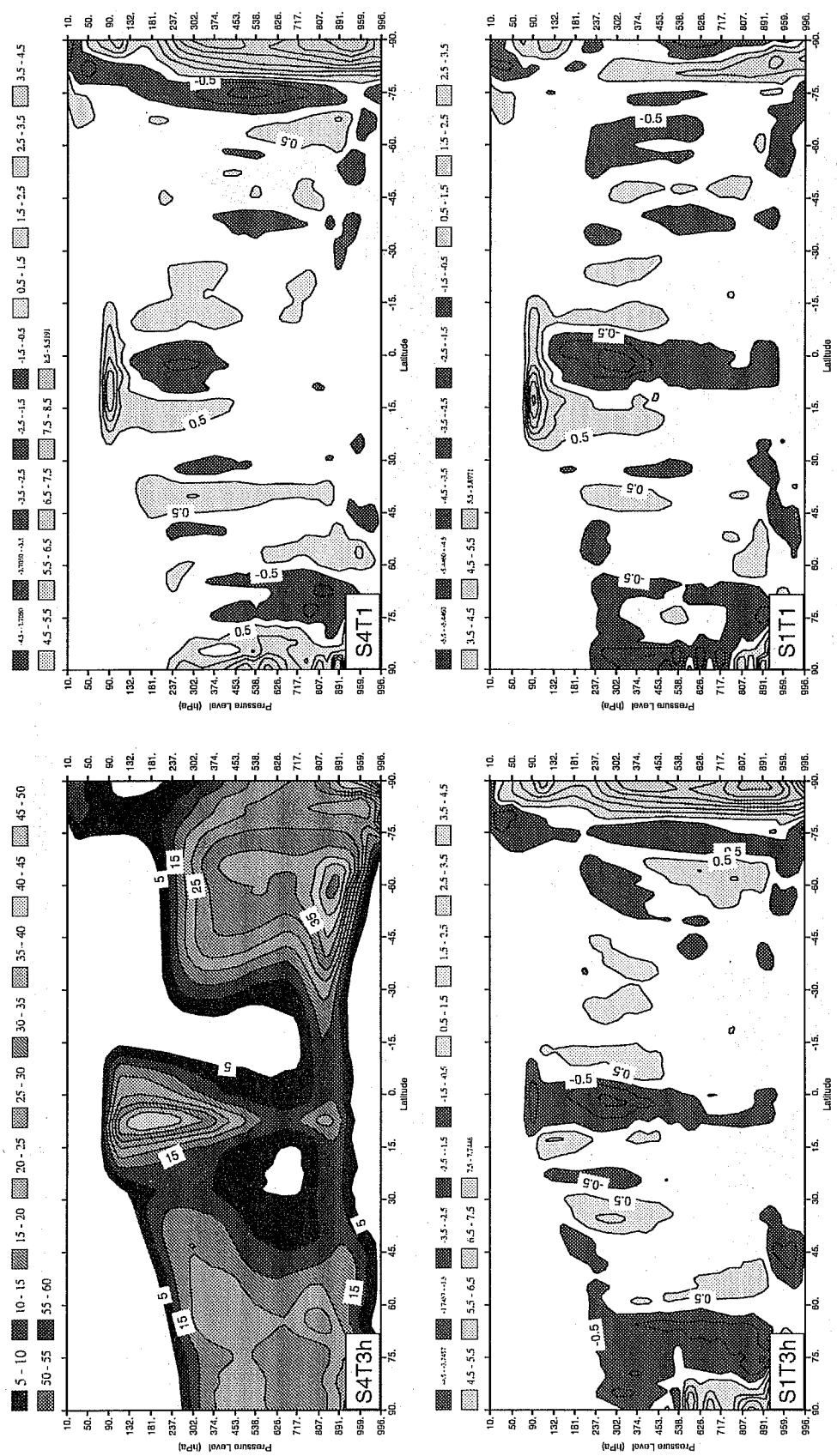

Figure 13: The zonal mean distribution of the cloud fraction averaged over the last 3 months of T_L95 L31 simulations (in percent). Top left panel is the operational configuration (S4T3h), top right is the difference S4T1-S4T3h, bottom left is the difference S1T3h-S4T3h bottom right is the difference S1T1-S4T3h.

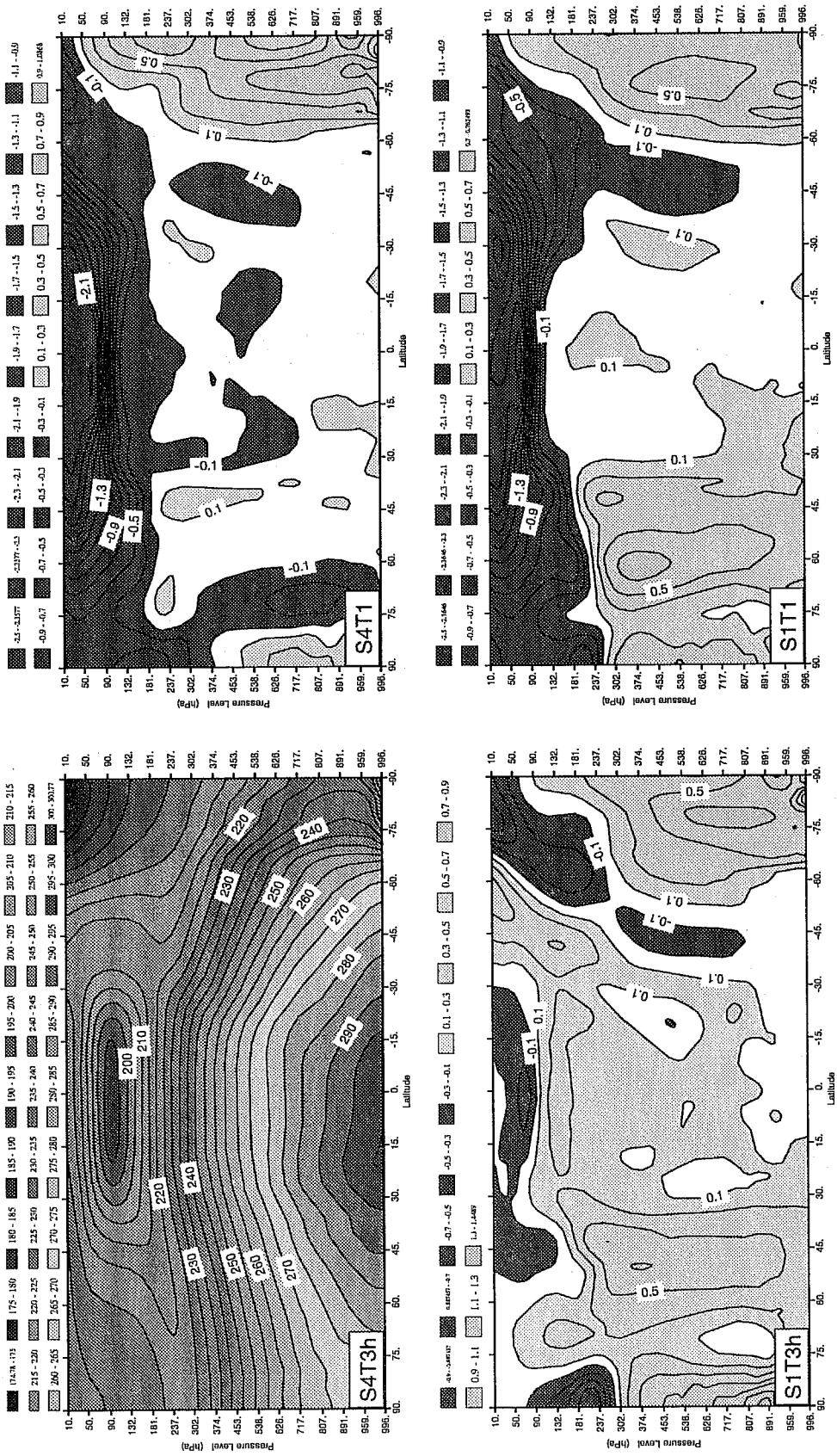

Figure 14: As in Figure 13, but for the zonal mean temperature (in degrees Kelvin).

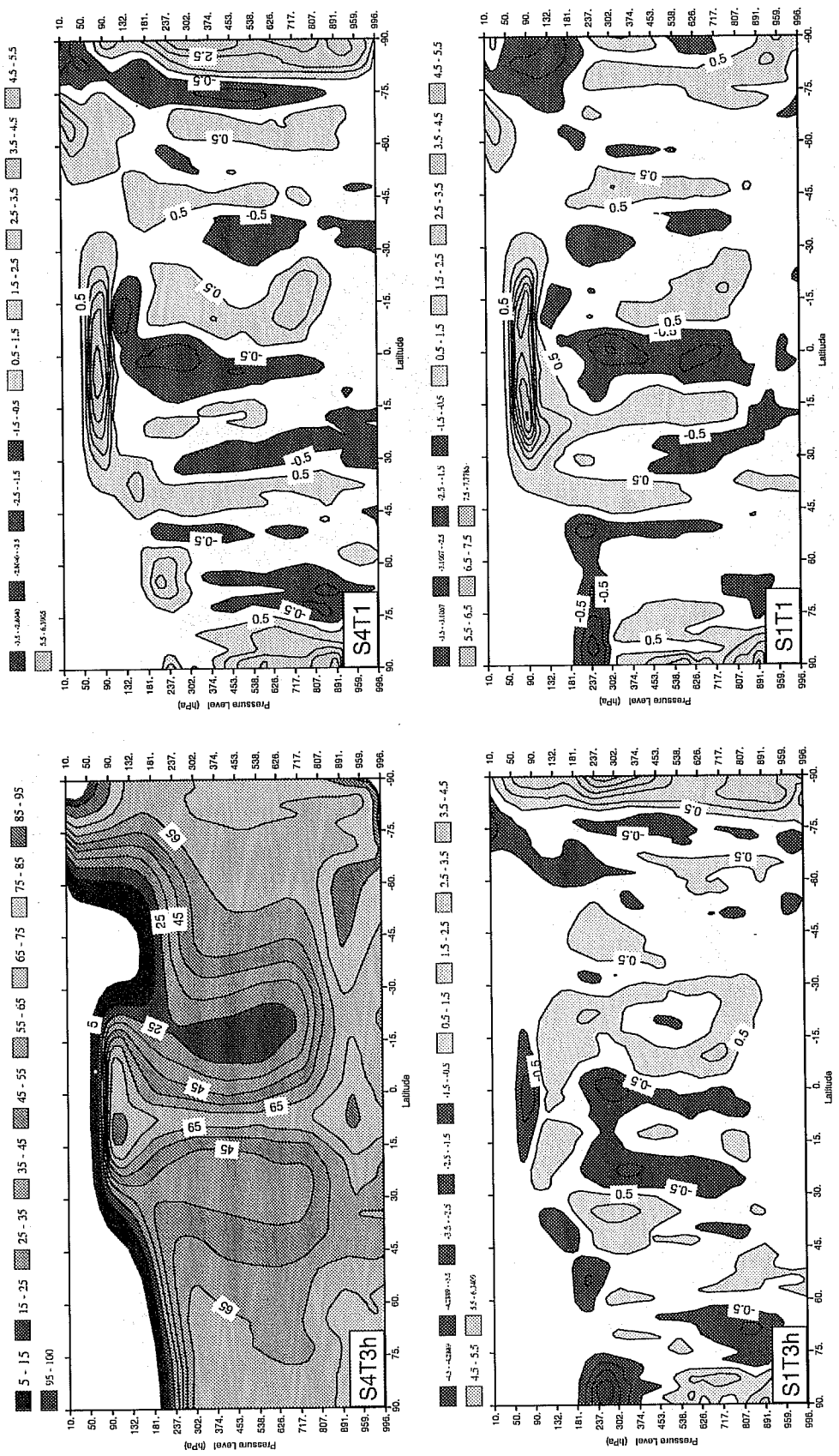

Figure 15: As in Figure 13, but for relative humidity (in percent).

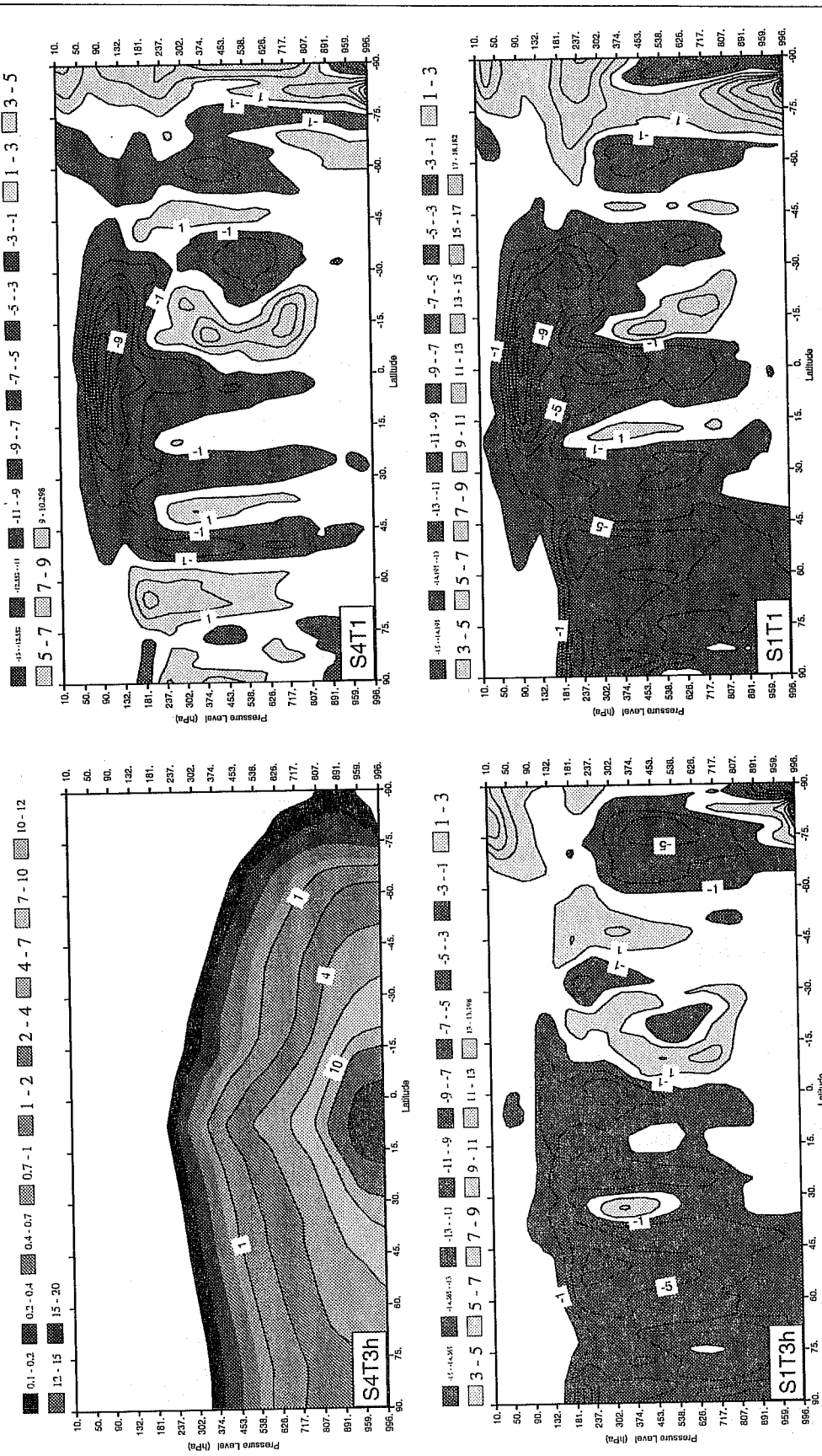

Figure 16: As in Figure 13, but for the specific humidity (in kg/kg). Differences are shown as Δq/q (in percent).

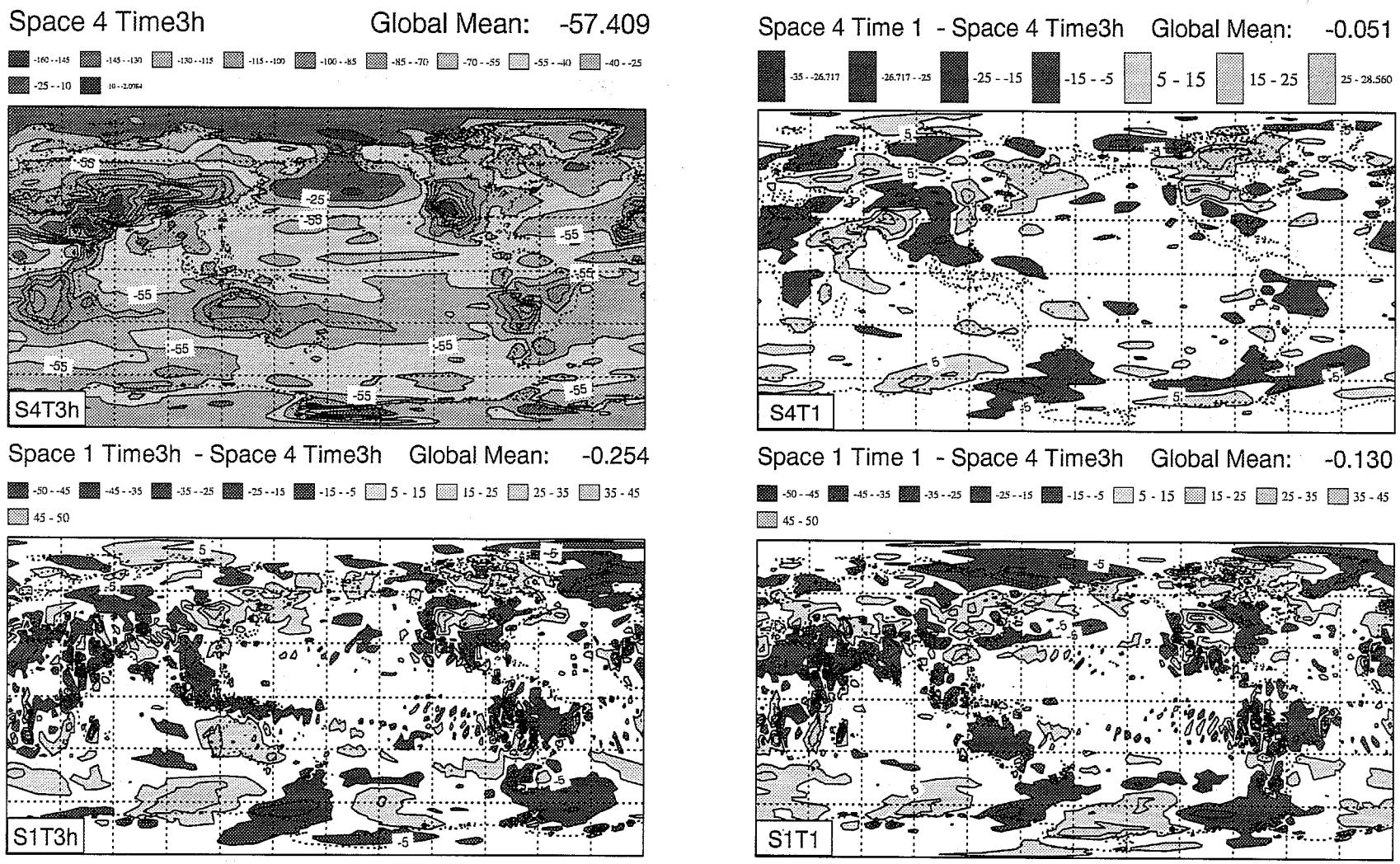

Figure 17a: The net longwave radiation at the surface for the 4 different radiation temporal/spatial configurations, within the T63 L31 model.

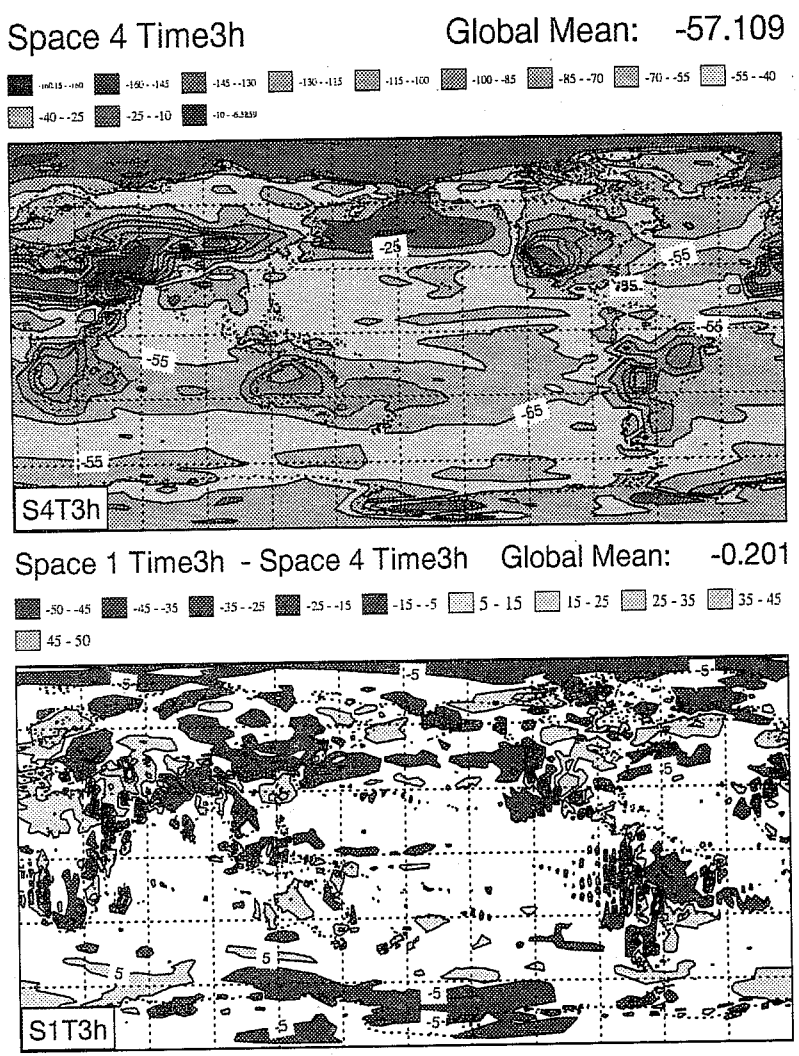

Figure 17b: As in Figure 17a, but for the T_L95 L31 model.

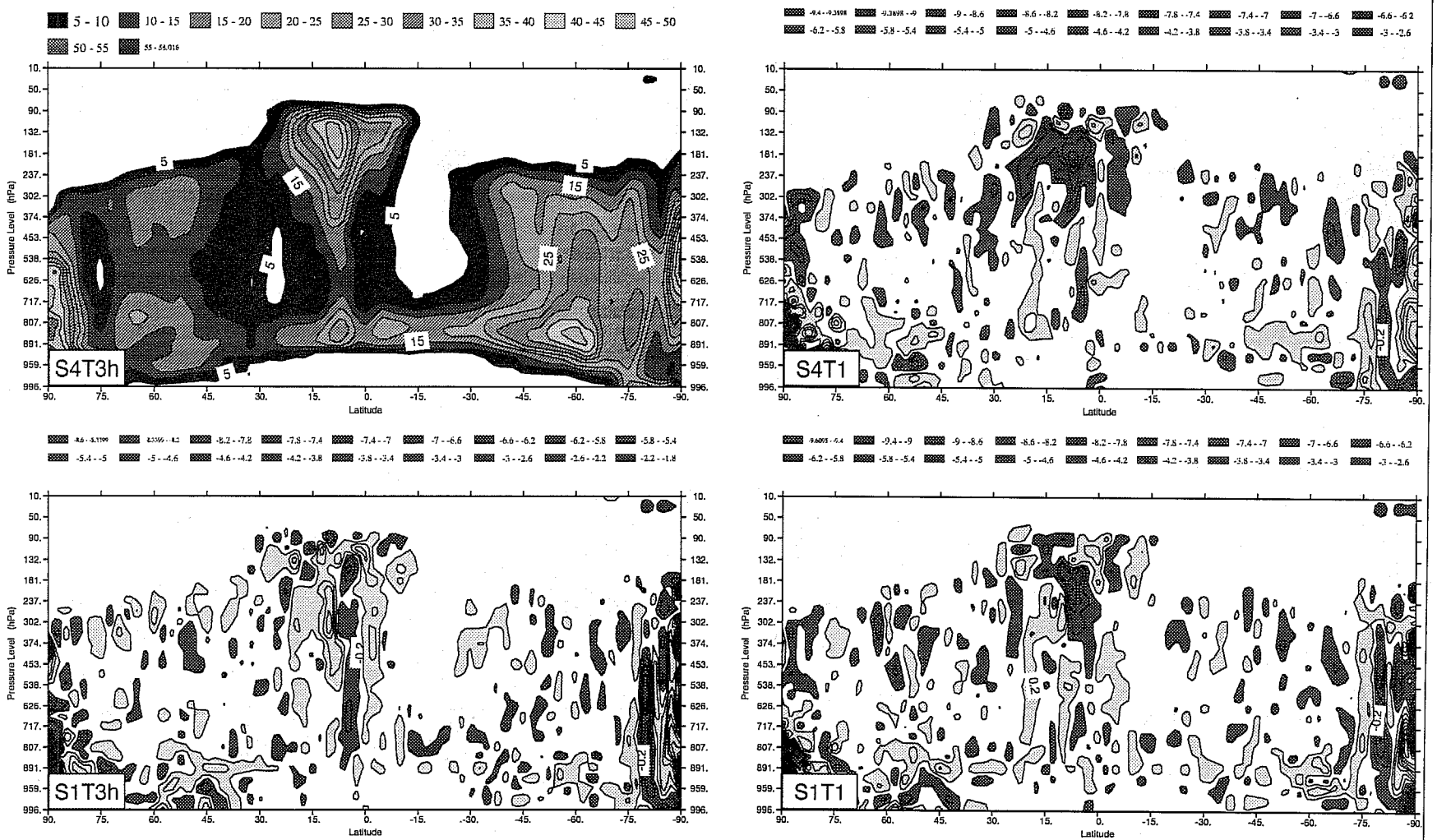

Figure 18: Impact of the various temporal/spatial radiation configurations on the cloud cover in the 6-hour first guess forecasts. The field is presented as a zonal mean, and averaged over 24 T_L319 L31 analyses, 6 hours apart from 19980701 00UTC.

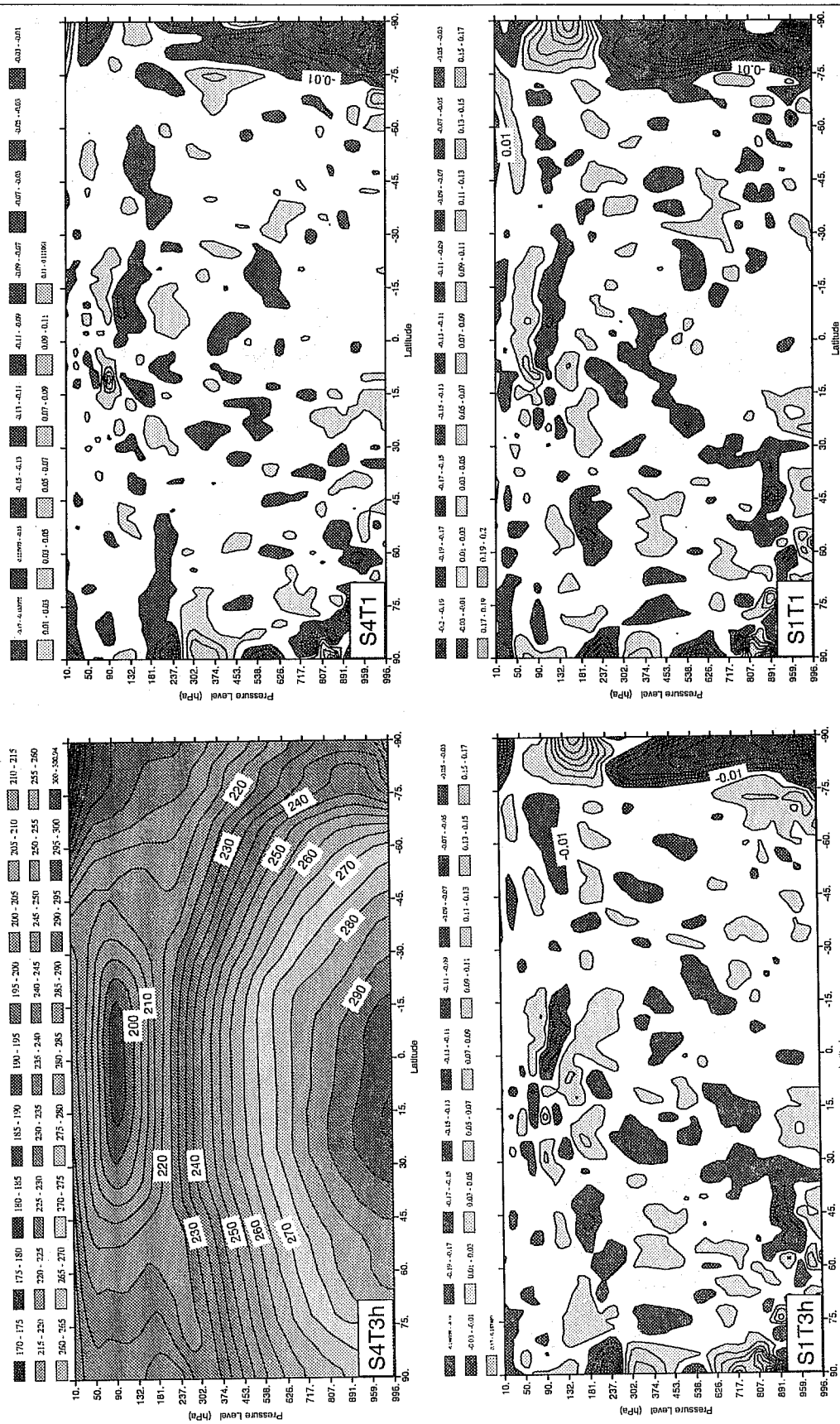

Figure 19: As in Figure 18, but for the analyzed temperature (in degrees Kelvin)

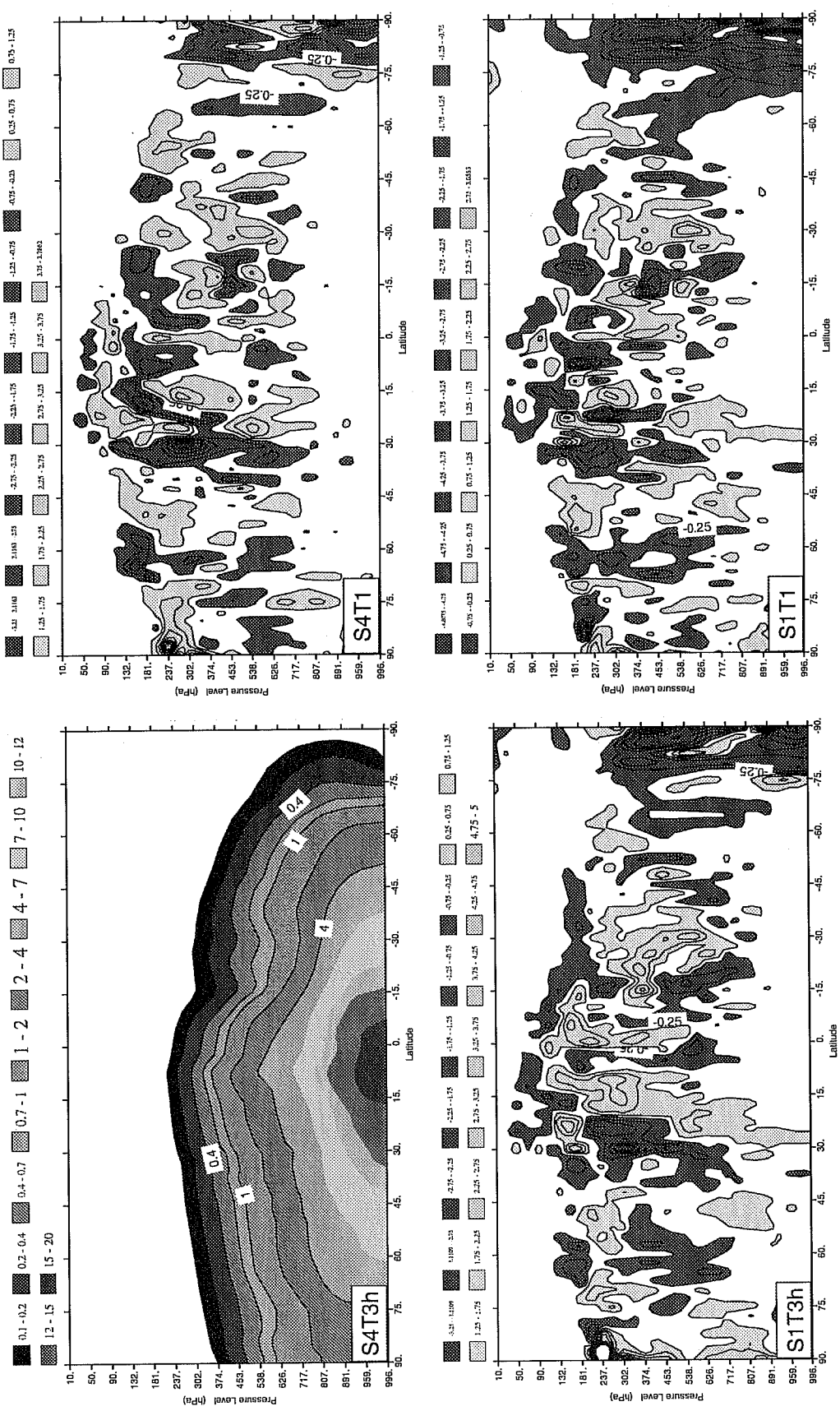

Figure 20: As in Figure 18, but for the analyzed specific humidity (in kg/kg). Difference panels show the relative difference Δq/q (in percent).